Chiroptical and magnetic properties of starshaped FeIII 4 complexes from chiral Schiff bases. Structural and magnetic correlations based on continuous shape measures†

Julia Mayans,[a] Mercè Font-Bardia[b] and Albert Escuer [*a]

a Departament de Química Inorgànica i Orgànica, Secció Inorgànica and Institute of Nanoscience and Nanotechnology (IN2UB), Universitat de Barcelona, Av. Diagonal 645, Barcelona-08028, Spain.
b Departament de Mineralogia, Cristal·lografia i Dipòsits Minerals and Unitat de Difracció de R-X. Centre Científic i Tecnològic de la Universitat de Barcelona (CCiTUB). Universitat de Barcelona, Solé i Sabarís 1-3, 08028 Barcelona, Spain

albert.escuer@ub.edu (A. Escuer).

ABSTRACT:

New chiral FeIII 4 star-shaped complexes have been synthesized starting from enantiomerically pure Schiff bases and chiroptically and magnetically characterized. The structural and magnetic properties of the complete family of 40 Fe4 complexes reported in the literature have been analyzed in the search for synthetic and magnetostructural correlations

INTRODUCTION

Fe4 star shaped clusters comprise an aesthetically pleasant family of complexes that show moderately strong antiferromagnetic interaction between the central and the three peripheral FeIII cations with an overall ferrimagnetic response and a well isolated S = 5 ground state. In spite of the 6S ground term of the high spin FeIII cations, they become moderately anisotropic by the distortion of the coordination polyhedron and usually exhibit slow relaxation of the magnetization. The starshaped topology has been reported from the employment of substituted tris(hydroxymethyl)ethane,1–13 alkoxides,14,15 N-methyldiethanolamine,16–18 Schiff bases19–25 and one isolated case from the tartrate ligand.26

After the discovery of the single molecule magnet (SMM) phenomenon in 1993,27–29 the complex [Fe4(MeO)6(dpm)6] (dpm = dipivaloylmethane) was studied early in 1999 by Gatteschi et al.14 and from the characterization of the [Fe4(thme)2(dpm)6] complex,1 in which dpm is the deprotonated form of the tripodal ligand tris(hydroxymethyl)ethane, a large number of [Fe4(R-thme)2(dpm)6] clusters (R-H3thme = substituted tris(hydroxymethyl)ethane) were synthesized and magnetically studied, becoming one of the most well-known families of SMMs. Fe4 complexes built from Schiff bases obtained by condensation of salicylaldehyde and 1,2-aminoethanol or their substituted derivatives have been reported more recently by S. Gao et al.21–23

These types of complexes with the formula [Fe4L6] become of interest because in addition to having similar magnetic properties and SMM response, they allow the possibility to modify the different substituents either on the aromatic ring or on the aliphatic C-atoms of the hydroxyethyl fragment. In the latter case, monosubstituted carbon atoms become chiral centres that open the possibility of incorporating optical properties or the study of chiral supramolecular effects.30–32

The employment of o-vanillin instead of salicylaldehyde remains unexplored with the exception of the Fe4 complex with the formula [Fe4(L)4(MeO)2Cl2] prepared with the Schiff base derived from 1,3-aminopropanol which yielded a very asymmetric complex, probably due to the large bite and steric hindrance of the propyl fragment.25 With this idea in mind, we decided to prepare enantiomerically pure Schiff bases derived from the condensation of o-vanillin and several chiral derivatives of 1,2-aminoethanol. Positive results were obtained for the ligands H2L1 (derived from (R)- or (S)-phenylglycinol) and H2L2 (derived from (1R,2S)-diphenylaminoethanol), Scheme 1, that allowed the characterization of a pair of starshaped enantiomers with the formula [Fe4(L1)6] (1R and 1S) and one mononuclear derivative of H2L2 with the formula [Fe(L2)(HL2)] (2RS). The tetranuclear systems have been characterized by electronic circular dichroism and static and dynamic susceptibility measurements. Bibliographic data show that the coordination polyhedral around the FeIII cations can vary from octahedral to trigonal prismatic; on the one hand, we have analyzed all the reported structures of the Fe4 complexes with star topology using SHAPE software and the continuous shape measures (CShM) as a tool to study the relationship between the ligands and the distortion of the coordination polyhedra around the FeIII cations and, on the other hand, have examined whether there is a correlation between

the aforementioned distortion of the coordination environment of the cations and the main magnetic parameters J and D or their SMM response.

EXPERIMENTAL

Materials and methods

IR spectra (4000–400 cm−1) were recorded using a Bruker IFS-125 FT-IR spectrometer with samples prepared as KBr pellets. Variable-temperature magnetic studies were performed using an MPMS5 Quantum Design magnetometer operating at 0.03 T in the 300–2.0 K range. Diamagnetic corrections were applied to the observed paramagnetic susceptibility using Pascal's constants. The fit of the experimental data was performed with the PHI program.33 The quality factor was parametrized with the parameter R = (χMTexp − χMTcalc)2/(χMTexp)2. EDC spectra were recorded in dichloromethane solution in a Jasco-815 spectropolarimeter.

Single-crystal X-ray crystallography

Red prism-like specimens of dimensions 0.055 mm × 0.130 mm × 0.213 mm (1R), 0.111 mm × 0.201 mm × 0.202 mm (1S) or 0.058 mm × 0.113 mm × 0.195 mm (2S) were used for X-ray crystallographic analysis. The X-ray intensity data were obtained on a D8 Venture system equipped with a multilayer monochromator and a Mo microfocus (λ = 0.71073 Å).

The frames were integrated with the Bruker SAINT software package using a narrow-frame algorithm. The final cell constants were based upon the refinement of the XYZ-centroids of reflections above 20 σ(I). The structure was solved and refined using the Bruker SHELXTL software package. Details of the crystal data, collection and refinement for 1R, 1S and 2RS are summarized in Table 1.

Synthetic procedure

[Fe4(L1)6]·solvents (1R·2CH2Cl2 and 1S·2MeCN). Complex 1S·2MeCN was accidentally crystallized in very low yield from a methanol/acetonitrile solution of FeCl2, LnCl3 and H2L in a basic medium during the trials to synthesize mixed iron/lanthanide complexes. In light of the structure, the direct synthesis was optimized to obtain complex 1R·2CH2Cl2 in a high yield. A solution of 0.5 mmol (0.069 g) of the corresponding (R) or (S)-phenylglycinol and 0.5 mmol (0.076 g) of o-vanillin in 15 mL of methanol was heated for 30 minutes at 80° in a microwave furnace. The yellow solution of the H2L ligand was added to 0.101 g (0.25 mmol) of Fe(NO3)3·9H2O dissolved in 10 mL of acetonitrile. The color of the solution turned to deep blue and changed immediately to dark red after the addition of 0.101 g (1.0 mmol) of Et3N. The mixture was stirred for 30 minutes and filtered to collect the complex as a brown microcrystalline powder in a practically quantitative yield. The crude complex was dissolved in 10 mL of dichloromethane and diffused with a vapour of diethyl ether. Well-formed crystals were collected after three days in 70% yield. IR spectra are shown in the ESI, Fig. S1.† Elemental analysis for 1R as a solvent free complex: calc. C, 62.69; N, 4.57; H, 4.93%. Found: C, 62.1; N, 4.4; H, 5.1%.

[Fe(L2)(HL2)2]·solvents (2RS). The ligand was prepared following the same procedure as that of H2L1 but starting from (1R,2S)-2-amino-1,2-diphenylethanol instead of phenylglycinol. To a methanolic

120 solution of 0.5 mmol of H2L2 were added 0.032 g (0.25 mmol) of anhydrous FeCl2 and 0.101 g (1
121 mmol) of Et3N. Slow evaporation of the final dark red solution gave crystals useful for X-ray diffraction
122 in a few days. Elemental analysis for 2RS: calc. C, 70.69; N, 3.75; H, 5.26%. Found: C, 70.3; N, 4.0; H,
123 5.3%.
124

RESULTS AND DISCUSSION

Structural description

[Fe4(L1)6]·solvents (1R·2CH2Cl2 and 1S·2MeOH). The two enantiomers were obtained with two molecules of different solvents, but the crystallization molecules are placed in the same voids in the network, and the two samples are isostructural, Table 1. The molecular structures of the tetrameric complexes show minor differences in their bond parameters, and thus to avoid repetitive descriptions, the following data refer to 1S.

The tetranuclear clusters consist of three peripheral [Fe(L1)2]− fragments that act as bidentate complex-as-ligand linking the central FeIII cation to form a star-shaped cluster, Fig. 1. The central FeIII ion is hexacoordinated by six bridging alkoxide donors that define a coordination polyhedron close to a trigonal prism, whereas the peripheral cations are placed in a distorted octahedral [FeN2O4] environment. A detailed analysis of the coordination polyhedron for the two environments is provided in the following sections. The Fe–O distances (range 1.924–2.075 Å) are shorter than the Fe–N distances (range of 2.114–2.159 Å), and thus the peripheral FeIII ions are slightly elongated along the N–Fe–N axis. The Fe–O–Fe bond angles are different for each peripheral cation, being shorter for Fe2–O–Fe3 (104.1/104.8°), larger for Fe2–O–Fe4 (108.0/109.0°) and intermediate for Fe2–O–Fe1 (104.4/107.3°). The four iron cations are placed in the same plane. The angles between the mean iron plane and the planes determined by the Fe–(O)2–Fe atoms (helical pitch) range between 77.2 and 83.9°. The main planes of the L12− ligands form a mean angle of around 56° with the Fe4 plane determining the propellershape of the cluster. Main bond parameters are summarized in Table 2.

[Fe(L2)(HL2)]·2MeCN·MeOH (2RS·2MeCN·MeOH). The mononuclear complex 2RS shows an FeIII cation in a distorted [FeN2O4] octahedral environment, coordinated by one deprotonated L22− and one monodeprotonated HL2− ligand, Fig. 2. Fe–O bond distances to the deprotonated O-donors are between 1.900 and 1.963 Å and are shorter than the distance to the protonated alkoxide (Fe–O4, 2.206 Å). As is usual for this type of ligands, the Fe–N distances are larger than 2.1 Å. The crystallization methanol molecule establishes a strong O1w···H4–O4 H-bond with an O4···O1w distance of 2.618 Å. Selected bond parameters are summarized in Table S1.†

Synthetic aspects

The reaction of H2L1 with iron nitrate in a basic medium yielded compounds 1R/1S, and in light of these results, similar reactions under the same conditions were tried with the Schiff bases derived from the condensation of o-vanillin and 2-amino-1-butanol or phenylalaninol. In contrast with compounds 1R/1S, the final products were soluble in the mother liquor, and no solid product was obtained upon layering with diethyl ether. All trials to obtain the solid complexes in a variety of solvents (methanol, acetonitrile, and dichloromethane) and by diffusion of diethyl ether or hexane gave oils. Susceptibility measurements performed on the crude product obtained by removing the solvent of the mother solution

show the typical shape expected for an Fe4 star but with a lower g value that evidences logical impurities.

The complexes derived from L12− exhibit a sand-glass shape with two cavities above and below the Fe4 plane, Fig. 3. The walls of the cavity are formed by the aromatic rings and the methoxide functions of the o-vanillin fragments with the aliphatic ethoxide bridging arm placed inside the cavity. This arrangement evidences that the –CH2– fragment fits inside the cavity but substitution of the H-atoms by a larger function must lead to a loss of the stability of the structure. The reaction with H2L2 with one phenyl group in this position effectively makes the Fe4 structure impossible, and the simple mononuclear complex was obtained, showing that this type of structure can be obtained with any substituent on the C-atom adjacent to the imine and that the aforementioned structures become impossible when the substitution is on the carbon adjacent to the O-donor.

Comparison with the structure of the related complex with the Schiff base without the methoxide group (L32−) (reported by S. Gao, CCDC code UVIPUL)21 shows that this substituent is not innocent. For this complex with the [Fe(L3)6] formula, there is enough free space to rotate the ligands giving a quasiperfect trigonal prism environment for the central FeIII cations, with a mean helical pitch of 88.5°. The steric hindrance produced by the methoxide substituent reduces the helical pitch to a mean value of 80.1°, distorting the environment of the FeIII cations and, as is explained in the following sections, has influence on its magnetic response.

Chirality transfer and electronic circular dichroism

The employment of chiral ligands in coordination chemistry usually induces the phenomenon of chirality transfer which produces structures with pre-determined supramolecular chirality that can be observed at several hierarchical levels, from the Λ/Δ absolute configuration of the coordination sphere of the cations to the arrangement of the molecule or the whole network.30–32

In our case, the transference of chirality in 1R/1S can be observed on the central cation that, in spite of its small deviation from the trigonal prism topology, shows the opposite distortion sense for each enantiomer, Fig. 4, top. The same feature occurs for the peripheral FeIII cations which show an octahedral environment and opposite configurations for the two enantiomers, Fig. 4, middle. The tilted planes of the L12−ligands with a main Fe4 plane determine, as was described above, the propeller-shape of the cluster which also shows opposite helicity for 1R and 1S, Fig. 4, bottom, resulting in a supramolecular helicate arrangement. The sense of the molecular helicity and the environments of the central and the three peripheral FeIII cations show a Δ configuration for 1R, whereas Λ is the configuration for the enantiomer 1S.

Electronic circular dichroism confirms the enantiomeric nature of 1R and 1S. The spectrum of 1R collected in dichloromethane solution exhibits positive Cotton effects at λmax = 244 and 398 nm and negative Cotton effects at 272, 312, 451 and 560 nm, whereas 1S shows a mirror image at the same wavelengths and with opposite sign, Fig. 5.

Several enantiomeric pairs of Fe4 clusters have been reported, but the dichroism studies are rare. S. Gao et al.21 reported the DFT simulation for several related [Fe4L6] complexes (L2− = Schiff bases derived from salicylaldehyde and phenylglycinol) as the sum of the contribution of L2− and the chirality transfer to the coordination spheres of the central and the peripheral FeIII cations, confirming that the intense absorptions below 300 nm are attributable to the chiral ligand, whereas the absorptions with the opposite Cotton effect around 300 and 400 nm have a main contribution from the central FeIII, and the bands above 450 nm are due to the peripheral cations and are attributed to d–d transitions and ligand to metal charge transfer. The close similitude above 300 nm of the spectra of 1R/1S with those previously reported gives a clear signature for this type of cluster with Schiff bases and the trigonal prism (central cation) and octahedral (peripheral cations) environments.

Magnetic properties

The χMT vs. T plot for complex 1R shows a room temperature value of 13.05 cm3 K mol−1, lower than the expected value of 17.50 cm3 K mol−1 for four non-interacting FeIII cations, each one with S = 5/2. On cooling, the χMT value decreases down to a minimum of 12.12 cm3 K mol−1 at 150 K and, below this temperature, increases up to a maximum value of 14.99 cm3 K mol−1 at 16 K and decreases to a final value of 13.96 cm3 K mol−1 at 2 K, Fig. 6. The shape of the plot and the χMT values indicate a ferrimagnetic-like behavior as a consequence of an anti-ferromagnetically coupled system without a full compensation of the spins.

The χMT decay at low temperatures can be either due to the anisotropy of the cations (zero field splitting in the S = 5 ground state) or antiferromagnetic intercluster interactions, which usually are strongly correlated in the fitting procedure.

On the basis of the coupling scheme shown in Fig. 6 (inset), in which J1 corresponds to the interaction between the central and peripheral FeIII cations and J2 parametrizes the weak interaction between the external cations and the derived Hamiltonian:

$$H = -2J_1(S_2 \cdot S_1 + S_2 \cdot S_3 + S_2 \cdot S_4) - 2J_2(S_1 \cdot S_3 + S_3 \cdot S_4 + S_1 \cdot S_4)$$

two independent fits were performed to simulate the experimental data, assuming that Dion = 0 and variable zJ intercluster interactions or variable Dion and zJ = 0. The fit neglecting the zero field splitting effect gave the best fitting values J1 = −9.6 cm−1, J2 = +1.3 cm−1, g = 2.01, and zJ = −0.0026 cm−1,whereas the fit assuming a D value different from zero and neglecting zJ yields gave the values J1 = −9.5 cm−1, J2 = +1.4 cm−1, g = 2.00, and D = 0.39 cm−1. The two fits were equally good and the fit curves were superimposable (R quality factors, 1.35 × 10−5 vs. 1.06 × 10−5), confirming that in this case, the fit of the susceptibility plot gives reliable values for the superexchange interactions but, in any case, can be applied to obtain an unambiguous approach to the D/zJ values.

To elucidate which is the dominant effect of the low temperature χMT decay, reduced magnetization experiments were performed, Fig. 7. In this case, the magnetization should be sensitive to the zero field splitting whereas, at medium-high fields, it becomes insensitive to very small intercluster zJ interactions. The reduced magnetization shows non-coincident plots for the explored fields and temperatures, and a satisfactory fit for all fields was obtained for D (ground state) = −0.29 cm−1, g = 1.98 and R = 6.2 × 10−5.

In light of the above data, the ground state should be described as S = 5 derived from the strong J1 interaction and with a moderately weak ground state anisotropy.

Alternate field (ac) susceptibility measurements performed at zero field do not show out-of-phase signals above 2 K, but measurements at 1000 Hz under transverse fields between 0 and 4000 G exhibit a strong dependence of the applied field, ESI Fig. S2,† evidencing strong quantum tunneling of magnetization. From these data, the static field of 1500 G was selected to perform the ac measurements in the 1488–200 Hz frequency range which shows frequency dependence signals corresponding to peak tails with the maxima below the lower temperature limit of the instrument, Fig. 8.

For well-defined signals for which the maxima of the peaks are not available and the Arrhenius law cannot be applied, the analysis of the data, assuming one relaxation process and one Ueff barrier, can be performed by means of the Debye relation:

$$\ln(\chi''_M/\chi'_M) = \ln(\omega\tau_0) - U_{eff}/k_BT$$

The fit of the experimental data for all frequencies except the lower one at 200 Hz that shows a too weak signal, Fig. 8, inset, gives a consistent set of values (ESI, Table S2†), and the mean parameters τ0 = 5.9 × 10−7 s and Ueff = 15.4 K in good agreement with the normal values found for these types of complexes.

Structural correlations

Despite the simplicity of the [Fe4(μ-O)6] core, the coordination environment of the FeIII cations exhibits large variations that are strongly dependent on the linking properties of the ligands. Continuous shape measures (CShM), proposed by Avnir and others,34,35 provide a quantitative evaluation of the degree of distortion from a given ideal polyhedron and, if there are two defined polyhedra, can evaluate it along the minimal distortion pathway that connects the ideal regular polyhedra. Parametrization of the coordination environments has been performed by means of the SHAPE program,36 which compares the real shape with the coordinates of the ideal polyhedron P, corresponding the S(P) = 0 value to the full agreement of the problem and the ideal coordinates.

The search in the CCDC database returns 40 Fe4 stars, but some of them correspond to pairs of enantiomers or structures measured at different temperatures, and thus the structural dataset was reduced to 35 independent structures. Shape measurements were performed for the central and peripheral iron

cations and the only close shapes were the octahedron (Oh) and the trigonal prism (TPr), and thus the minimal distortion pathway between these structures was selected for the analysis, the extreme points being S(Oh) = 0 and S(TPr) = 16.737 for an ideal octahedron and S(Oh) = 16.737 and S(TPr) = 0 for the ideal trigonal prism. For the systems that follow the distortion path, the structure is intermediate between the ideal polyhedra, whereas deviations from the path indicate other distortions (elongation, compression, short or long bond angles as a consequence of the bite of the ligands, etc.). The 35 structures have been classified into eight groups as a function of the ligands that are involved in the Fe–O–Fe bonds. The S(P) values are summarized in the ESI, Table S3.†

Practically one half of the Fe4 ferric stars (16 structures, type I) are built from the tripodal ligand tris(hydroxymethyl) ethane (H3thme) or a variety of the R-substituted ligand (R-H3thme) and acetylacetonate or dipivaloylmethane (R-acac) to fulfill the remaining coordination sites of the peripheral FeIII, with the general formula [Fe4(R-thme)2(R-acac)6], Scheme 2.

Also, with acetylacetonate peripheral ligands we have the type II (one structure) with the formula [Fe4(R-thme)(EtO)3(Racac) 6] and type III (two structures) with the formula [Fe4(Meo)6(R-acac)6].

Four complexes were derived from N-methyldiethanolamine (H2mdea) with the formula [Fe4(mdea)6] (type IV) and from Schiff bases (H2Schiff) were derived from the condensation of salicylaldehyde with 2-aminophenol (two structures, type V) or 2-aminoethanol or their 2-R-substituted analogues (six structures, type VI) with the [Fe4(Schiff)6] formula. Finally, one system with one reduced Schiff base with the same [Fe4(L)6] formula (type VII) and three complexes with very asymmetric cores (type VIII) complete the set of structures.

The SHAPE analysis of the central FeIII cations shows a wide distribution of their coordination environments from the octahedral shape for type V to quasi-perfect trigonal prisms for the Schiff base derivatives, type VI, Fig. 9. The shape of the coordination polyhedra follows the Oh–TPr minimal pathway, revealing that this type of distortion becomes the most relevant for all the Fe4 stars. In particular, the most studied series I and VI fit quasi-perfectly on the pathway. Other distortions become relevant for the octahedral II–V and VII complexes, with very close shape characteristics for each kind of ligand.

In particular, the steric hindrance promoted by the methoxide group in 1R/1S, Fig. 3, induces a larger distortion from the trigonal prism environment around the central cation for the type VI complexes.

The same analysis for the peripheral FeIII cations shows that the distorted octahedron is the preferred environment in most of the cases, but with the exception of the type I–III complexes that follow the Oh–TPr pathway, and the remaining systems show important distortions related with the donor properties of the coordinated ligands, Fig. 10. In fact, for type I, the two acetylacetonate ligands coordinated to the iron cations provide a comfortable bite angle (∼85°) that favors a low distorted octahedral arrangement, whereas, for types IV and VII, the fac-coordination of the tridentate ligands with bite angles ∼75–79° determine very distorted environments that are relatively close to the trigonal prism.

It is worth noting that, for the two larger series I and VI, for which there are enough complexes to extract conclusions, we realize that the environment of the peripheral cations for type I is quasi-constant with an S(Oh) in the short range 0.79–1.31 for the complexes derived from the rigid Schiff bases (type VI), and there is a clear correlation between the degree of S(TPr) of the central cation and the distortion of the octahedral environment of the peripheral cations, that is to say, the more prismatic the central cation, the more octahedral the peripheral FeIII cations become, Table S3 and Fig. S3.†

One of the most interesting conclusions of this analysis is that each type of ligand produces, either for the central or the peripheral cations, Fe4 stars with a well-defined environment, and that the coordination around the FeIII cations for new members of the aforementioned structural types can be effectively predicted with a low margin of surprise by the adequate selection of the ligands.

Magnetic correlations. The main structural and magnetic parameters for the 30 complexes for which there is available information in the literature are summarized in Table 3. This series of complexes is specially adequate to analyze magnetostructural correlations because they are quite an unusual case in which the magnetic parameters are highly reliable: the value of the J coupling constants is a function, with low error margin, of the position of the minimum of χMT,and the D parameter has been determined in practically all cases from reduced magnetization or/and high field EPR. From these data, two independent correlations can be obtained, one for the J coupling constant between the central and peripheral cations and a second for their SMM response.

The superexchange between FeIII cations mediated by oxo bridges shows a moderate dependence of the bond angle (larger interactions for larger angles) and a strong dependence of the Fe–O distances in the bridging region (larger interactions for shorter distances) and several empirical methods have been proposed to predict the magnitude of the FeIII–O–FeIII interaction.37,38 From these models, it can be seen that few degrees of difference (102–106° range as an example) in the Fe–O–Fe bond angle are poorly relevant and suppose an increment of less than 1.5 cm−1 in the J value whereas the magnitude of the interaction changes drastically in the 1.95–2.05 range for the Fe–O distance. On this basis, a simple inspection of Table 3 shows that complexes with similar bond parameters have different J values and that the larger interactions correspond to the systems with Fe–O bond distances larger than 2.0 Å, and thus the reported complexes do not follow these well-established correlations. In the same way, there is no correspondence between the S(Oh) (central or peripheral cations) and the J parameter, ESI, Fig. S4.† This fact is not surprising because the magnitude of the superexchange interaction between the central and the peripheral cations of the Fe4 systems must be assumed as a complicated multifactor problem that, in addition to bond lengths and angles at the bridging region, includes the donor properties of each type of O-donor (alcoxo, phenoxo, etc.) and the extreme differences in the stereochemistry around the cations with the concomitant change of the atomic orbitals that participate in the superexchange pathway, from dx2 − y2/dz2 for an ideal octahedron (Oh, eg) to dxz/dyz for an ideal trigonal prism (D3h, e″) environments.

However, some general conclusions can be drawn from the experimental evidence: (a) the J parameter is coherent and characteristic for each type of compound following the order of the AF interaction type I ~ V < II ~ III < VI ~ VII. This means that the Schiff bases with alkoxo bridging arms promote larger interactions than the phenoxo ones and that the intermediate interactions correspond to the complexes with MeO− or EtO− bridges, Table 3. The only complex that does not follow this order is one type III system with a low J value attributable to the larger electronegativity of the fluorinated dipivaloylmethane ligands, and all type VIII complexes which show extreme asymmetric environments or even square pyramidal penta-coordination for the peripheral cations.

The dependence of D with the structural distortion of the octahedral polyhedron was studied by Gatteschi et al., proposing that the trigonal compression of the octahedron along the C3 axis contributes to larger and negative D values and that the trigonal rotation (from Oh towards TPr) also contributes to negative D values.14,39

Type I complexes have been exhaustively studied by R. Sessoli and others1–13 and the D parameter has been correlated to several distortion parameters such as the trigonal compression, trigonal rotation or the helical pitch defined as the dihedral angle between the main Fe4 and the Fe–(O2)–Fe planes. This latter parameter joins with the trigonal compression (larger pitch means lower compression) and trigonal rotation (larger pitch means larger rotation) and proved to be useful in a series of twelve type I complexes.7 For this type of complexes, with the same dipivaloylmethane ligands coordinated to the peripheral cations and a very similar Oh environment for the central FeIII cations placed on the distortion pathway (triangles in Fig. 9 and 10), the parameter S(Oh) joins both distortions and consequently yields to the same conclusion, it is to say, larger negative D for larger S(Oh), Fig. 11.

The trial to extend the correlation obtained for the homogeneous series of type I complexes to types II and III fails as was pointed out by the same authors and others.7,25 If the relationship is extended to all Fe4 types, the lack of correspondence between both parameters becomes evident. This fact seems logical because, as occurs for the J parameter, the correlation fails due to multiple factors that can tune the D parameter as a consequence of the completely different coordination polyhedron for the central and/or the peripheral cations. In fact, larger D values (~0.4 cm−1) are provided for type I complexes with intermediate/Oh environments for the central/peripheral cations and lower values (~0.2 cm−1) with a similar environment for type III, whereas similar D values of around ~0.3 cm−1 are found for completely different coordination polyhedra such as intermediate/Oh (type II), TPr/intermediate (type VI) or highly distorted as type VIII. On the other hand, it becomes evident that each type of complex possesses a characteristic D value.

A final aspect concerns the SMM response and particularly the Ueff barrier calculated for these complexes. In a quasi-systematic fashion, type I complexes exhibit $\chi''M$ peaks at zero field and above 2 K (typically between 2 and 3 K), whereas the other types, and in particular, those derived from Schiff bases (type VI) show peaks clearly below 2 K and, in some case even with the application of a static field to suppress the quantum tunneling of magnetization, do not overcome this temperature. In the same

way, the Ueff values for type I agree in general terms with the DS2 value but much lower values have been reported for the other types measured at zero field, confirming the large tunneling of the magnetization.

As a consequence of the steric restrictions for 1R/1S, the new compounds show larger distortion from the regular trigonal prism for the type VI complexes, showing low J and D values in comparison with the rest of the members of the family of [Fe(L)6] (L = Schiff base) complexes.

CONCLUSIONS

Two new tetranuclear, star-shaped FeIII complexes derived from enantiomerically pure Schiff bases obtained by the reaction of o-vanillin and phenylglycinol have been characterized. EDC spectra confirm characteristic peaks and the sign for the systems with the central cation in a trigonal prism environment. Magnetic analysis reveals an SMM response with a moderate D value and large tunneling. The previously published Fe4 complexes with the same topology have been reviewed in light of continuous shape measures with SHAPE software for eight types of Fe4 clusters, concluding that there are predetermined coordination environments for the central and peripheral FeIII cations for each type of ligand reported to date. In the same way, the distortion parameter S(Oh) proved to be adequate to establish structural and magnetic correlations for these types of complexes and J and D values are strongly dependent on the employed ligands, showing characteristic values for each type of complex and allowing the design of future clusters with predetermined magnetic properties.

ACKNOWLEDGEMENTS

Financial support from the Ministerio de Economía y Competitividad-Spain, Project CTQ2015-63614-P is acknowledged.

REFERENCES

1 A. Cornia, A. C. Fabretti, P. Garrisi, C. Mortalo, D. Bonacchi, D. Gatteschi, R. Sessoli, L. Sorace, W. Wernsdorfer and A. L. Barra, Angew. Chem., Int. Ed., 2004, 43, 1136.

2 S. Accorsi, A. L. Barra, A. Caneschi, G. Chastanet, A. Cornia, A. C. Fabretti, D. Gatteschi, C. Mortalo, E. Olivieri, F. Parenti, P. Rosa, R. Sessoli, L. Sorace, W. Wernsdorfer and L. Zobbi, J. Am. Chem. Soc., 2006, 128, 4742.

3 A. L. Barra, F. Bianchi, A. Caneschi, A. Cornia, D. Gatteschi, L. Gorini, L. Gregoli, M. Maffini, F. Parenti, R. Sessoli, L. Sorace and A. M. Talarico, Eur. J. Inorg. Chem., 2007, 4145.

4 G. G. Condorelli, A. Motta, G. Pellegrino, A. Cornia, L. Gorini, I. L. Fragala, C. Sangregorio and L. Sorace, Chem. Mater., 2008, 20, 2405.

5 A. Cornia, L. Gregoli, C. Danieli, A. Caneschi, R. Sessoli, L. Sorace, A. L. Barra and W. Wernsdorfer, Inorg. Chim. Acta, 2008, 361, 3481.

6 L. Bogani, C. Danieli, E. Biavardi, N. Bendiab, A. L. Barra, E. Dalcanale, W. Wernsdorfer and A. Cornia, Angew. Chem., Int. Ed., 2009, 48, 746.

7 L. Gregoli, C. Danieli, A. L. Barra, P. Neugebauer, G. Pellegrino, G. Poneti, R. Sessoli and A. Cornia, Chem. –Eur. J., 2009, 15, 6456.

8 C. Schlegel, J. van Slageren, M. Manoli, E. K. Brechin and M. Dressel, Polyhedron, 2009, 28, 1834.

9 C. Schlegel, E. Burzuri, F. Luis, F. Moro, M. Manoli, E. K. Brechin, M. Murrie and J. van Slageren, Chem. – Eur. J., 2010, 16, 10178.

10 M. J. Rodriguez-Douton, A. Cornia, R. Sessoli, L. Sorace and A. L. Barra, Dalton Trans., 2010, 39, 5851.

11 T. K. Prasad, G. Poneti, L. Sorace, M. J. Rodriguez-Douton, A. L. Barra, P. Neugebauer, L. Constantino, R. Sessoli and A. Cornia, Dalton Trans., 2012, 41, 8368.

12 A. Nava, L. Rigamonti, E. Zangrando, R. Sessoli, W. Wernsdorfer and A. Cornia, Angew. Chem., Int. Ed., 2015, 54, 8777.

13 M. Moragues-Canovas, E. Riviere, L. Ricard, C. Paulsen, W. Wernsdorfer, G. Rajaraman, E. K. Brechin and T. Mallah, Adv. Mater., 2004, 16, 1101.

14 A. L. Barra, A. Caneschi, A. Cornia, F. Fabrizi de Biani, D. Gatteschi, C. Sangregorio, R. Sessoli and L. Sorace, J. Am. Chem. Soc., 1999, 121, 5302.

15 L. Rigamonti, M. Piccioli, A. Nava, L. Malavolti, B. Cortigiani, R. Sessoli and A. Cornia, Polyhedron, 2017, 128, 9.

16 R. W. Saalfrank, I. Bernt, M. M. Chowdhry, F. Hampel and G. B. M. Vaughan, Chem. – Eur. J., 2001, 7, 2765. 17 R. W. Saalfrank, A. Scheurer, I. Bernt, F. W. Heinemann, A. V. Postnikov, V. Schunemann, A. X. Trautwein, M. S. Alam, H. Rupp and P. Muller, Dalton Trans., 2006, 2865.

18 S. Mishra, E. Jeanneau, M. Rolland and S. Daniele, RSC Adv., 2016, 6, 1738.

19 K. Takahashi, K. Kawamukai, T. Mochida, T. Sakurai, H. Ohta, T. Yamamoto, Y. Einaga, H. Mori, Y. Shimura, T. Sakakibara, T. Fujisawa, A. Yamaguchi and A. Sumiyama, Chem. Lett., 2015, 44, 840.

20 A. K. Dutta, S. Biswas, S. Dutta, L. N. Dawe, C. Robert Lucas and B. Adhikary, Inorg. Chim. Acta, 2016, 444, 141.

21 Y.-Y. Zhu, X. Guo, C. Cui, B.-W. Wang, X.-M. Wang and S. Gao, Chem. Commun., 2011, 47, 8049.

22 Y.-Y. Zhu, T.-T. Yin, S.-Da Jiang, A.-L. Barra, W. Wernsdorfer, P. Neugebauer, R. Marx, M. Dorfel, B.-Wu Wang, Z.-Q. Wu, J. van Slageren and S. Gao, Chem. Commun., 2014, 50, 15090.

23 Y.-Y. Zhu, C. Cui, K. Qian, J. Yin, B.-W. Wang, Z.-M. Wang and S. Gao, Dalton Trans., 2014, 43, 11897.

24 R. Singh, A. Banerjee, E. Colacio and K. K. Rajak, Inorg. Chem., 2009, 48, 4753.

25 N. T. Madhu, J.-K. Tang, I. J. Hewitt, R. Clerac, W. Wernsdorfer, J. van Slageren, C. E. Anson and A. K. Powell, Polyhedron, 2005, 24, 2864.

26 Q. Gao, X. Wang, M. T. Conato, T. Makarenko and A. J. Jacobson, Cryst. Growth Des., 2011, 11, 4632.

27 R. Sessoli, H. L. Tsai, A. R. Schake, S. Wang, J. B. Vincent, K. Folting, D. Gatteschi, G. Christou and D. N. Hendrickson, J. Am. Chem. Soc., 1993, 115, 1804.

28 R. Sessoli, D. Gatteschi, A. Canesch and M. A. Novak, Nature, 1993, 365, 141.

29 D. Gatteschi, A. Caneschi, L. Pardi and R. Sessoli, Science, 1994, 265, 1054.

30 J. Crassous, Chem. Soc. Rev., 2009, 38, 830.

31 H. Miyake, Symmetry, 2014, 6, 880.

32 M. Liu, L. Zhang and T. Wang, Chem. Rev., 2015, 115, 7304.

33 N. F. Chilton, R. P. Anderson, L. D. Turner, A. Soncini and K. S. Murray, J. Comput. Chem., 2013, 34, 1164.

34 S. Zabrodsky, D. J. Peleg and D. J. Avnir, J. Am. Chem. Soc., 1992, 114, 7843.

35 J. Cirera, P. Alemany and S. Alvarez, Chem. – Eur. J., 2004, 10, 190.

36 M. Llunell, D. Casanova, J. Cirera, P. Alemany and S. Alvarez, SHAPE version 2.0, Barcelona, 2010, the program can be obtained by requesting the authors.

37 S. M. Gorun and S. J. Lippard, Inorg. Chem., 1991, 30, 1625.

38 K. J. Mitchell, K. A. Abboud and G. Christou, Inorg. Chem., 2016, 55, 6597.

39 D. Gatteschi and L. Sorace, J. Solid State Chem., 2001, 159, 253.

Legends to figures

Scheme 1. Structural formula of the Schiff bases employed in this work and the coordination mode for L12− in the star-shaped Fe4 complexes. Asterisks denote the chiral centres.

Figure. 1 Partially labeled plot of complex 1S (common labels for 1R).

Figure..2 Partially labeled plot of complex 2RS. The dotted line shows the H-bond between HL− and the crystallization methanol molecule.

Figure.3. ECD spectra for complexes 1R (blue line) and 1S (red line). (Color online Left, axial view of complexes 1R or 1S showing the C-atoms of the methoxide functions (pink colour) and the C-atoms adjacent to the O-donor of the aliphatic arm (green color). Right, the same view for the analogous complex built from the related Schiff base without the methoxide substituent (CCDC: UVIPUL)..

Figure.4 Chirality transfer to the central (top) and peripheral (middle) FeIII cations in complexes 1R (left) and 1S (right). The same Λ or Δ helicity is transferred to the whole complexes (bottom).

Figure.5 Dichloromethane solution ECD spectra for the pair of Fe4 enantiomers (black line, 1R; red line, 1S).

Figure.6 χMT vs. T plot for complex 1R. The superimposed red or green continuous lines show the best fit obtained simulating the low T decay from intermolecular interactions or D effect (see text). Inset, coupling scheme.

Figure.7 Reduced magnetization plots in the 1.8–6.8 K range with 1 K increment for complex 1R. Solid lines show the best fit assuming an S = 5 ground state.

Figure.8 Alternate current out-of-phase susceptibility plot vs. T for complex 1R. Inset, natural logarithm of χ''/χ' vs. 1/T for the indicated frequencies.

Scheme 2 Structural types of the Fe4 stars reported in the literature as a function of the ligands that provide the Fe–O–Fe bridges.

Figure.9 S(TPr) vs. S(Oh) for the central FeIII cation of the 35 Fe4 independent structures reported to date. (I)–(VIII) refer to the structural types described in Scheme 2. The distortion pathway between the octahedral and the trigonal prism is shown as a solid black line.

Figure.10 S(TPr) vs. S(Oh) for the peripheral FeIII cations (mean values) of the 35 Fe4 independent structures reported to date. (I)–(VIII) refer to the structural types described in Scheme 2. The distortion pathway between the octahedral and the trigonal prism is shown as a solid black line.

Figure.11 D vs. S(Oh) of the central FeIII cation for the I, II, III, IV and VI type complexes. The solid line shows the tendency for type I complexes.

525 **SCHEME 1**

526

527

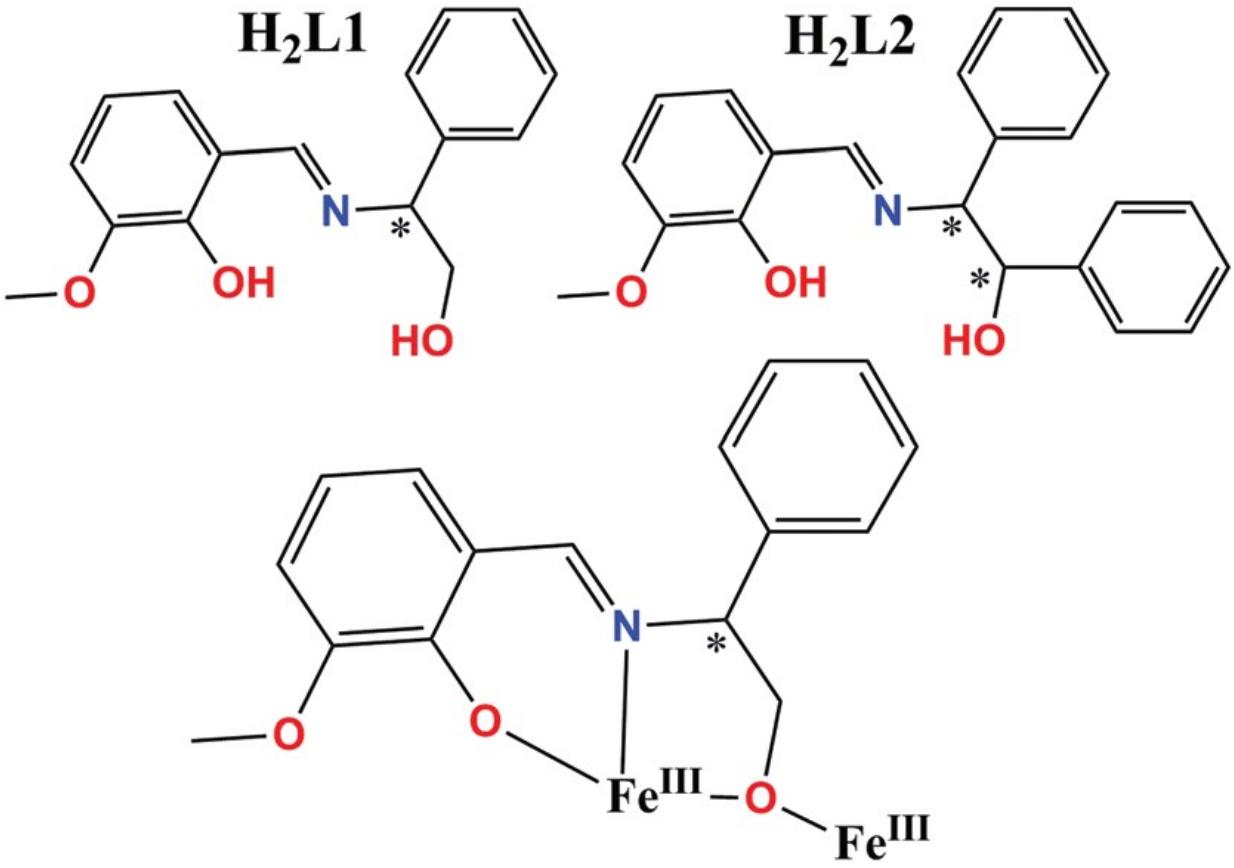

528

529

FIGURE 1

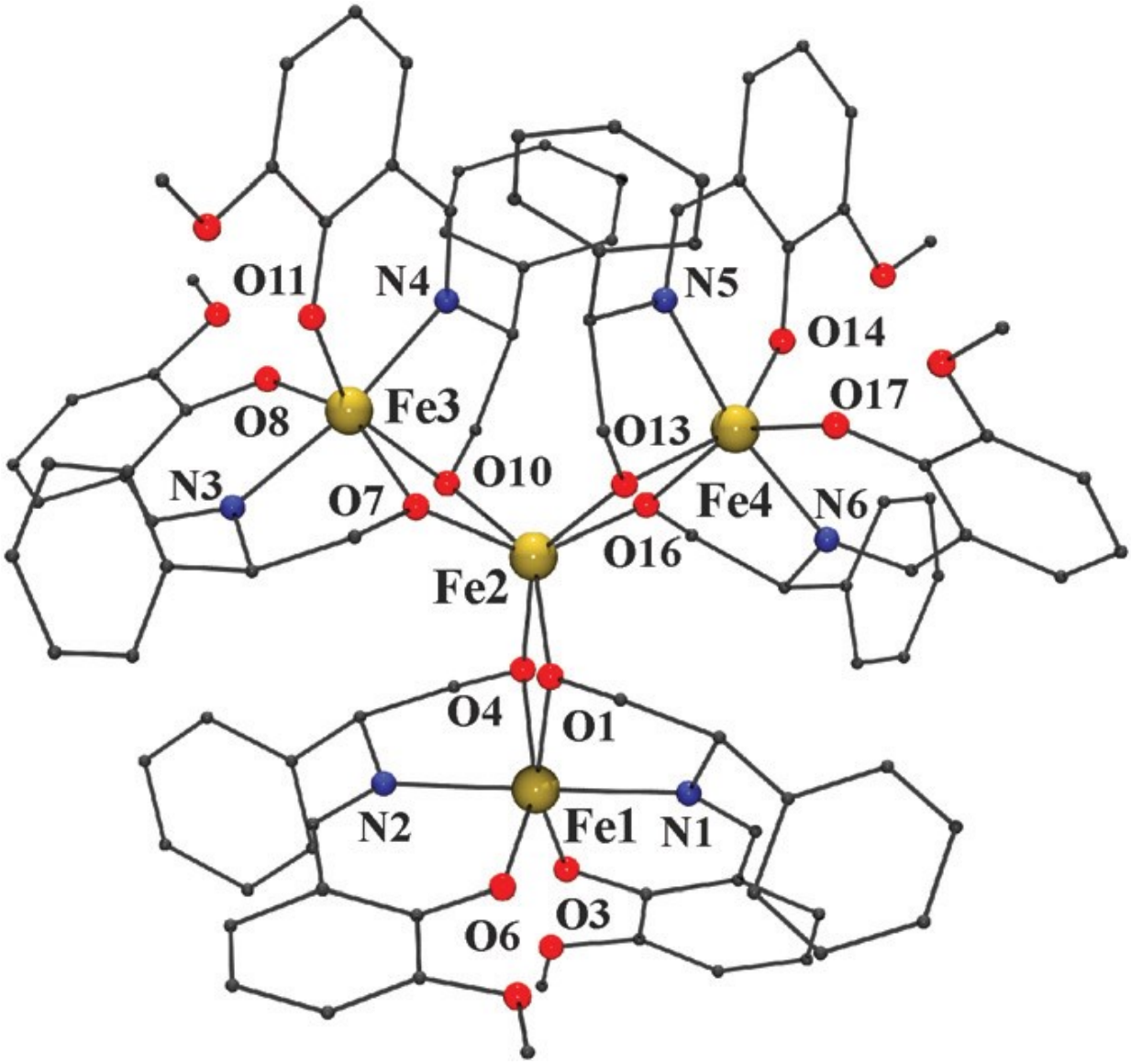
O11
N4
N5
O14
O8
Fe3
O17
O13
N3
O7
O10
Fe4
N6
O16
Fe2
O4
O1
N2
Fe1
N1
O6
O3

538 **FIGURE 2**

539

540

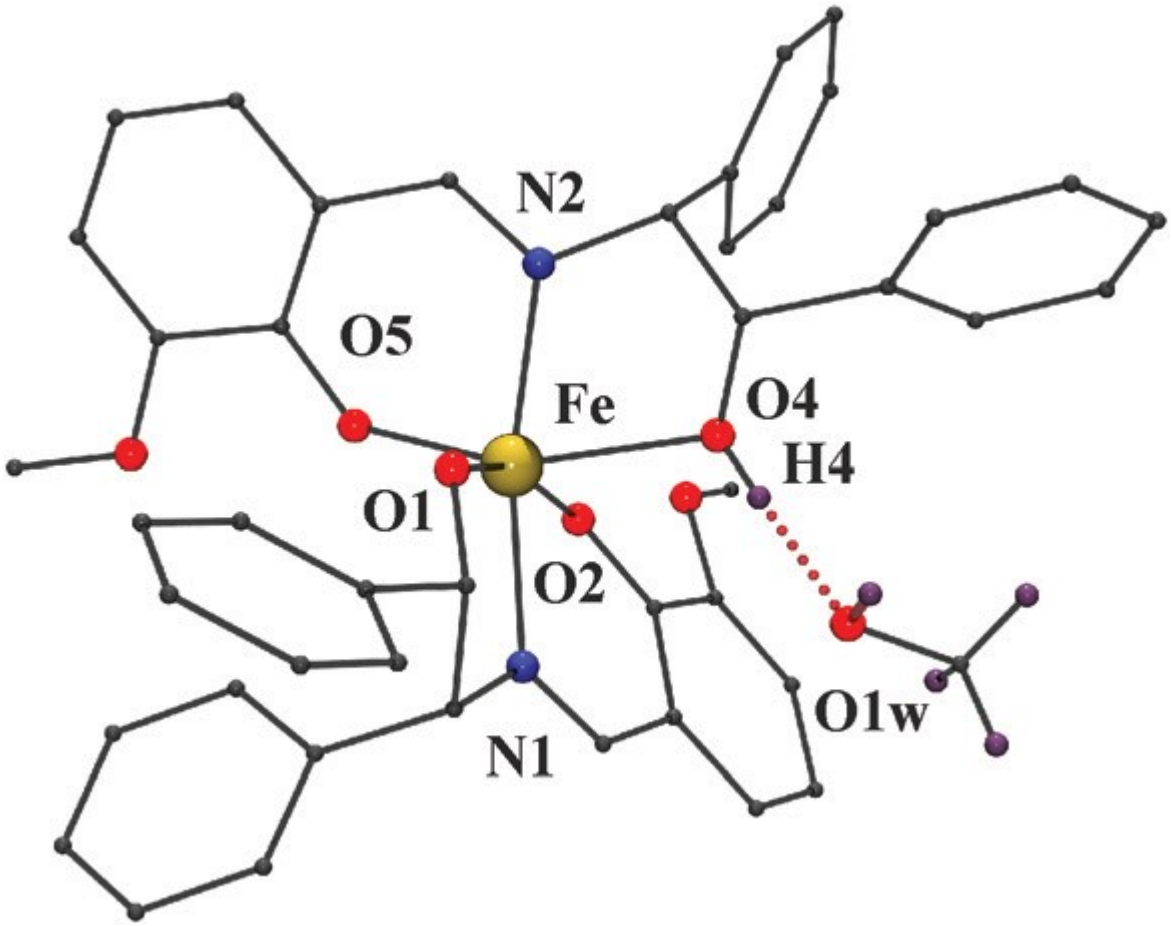

541

542

543 **FIGURE 3**

544

545

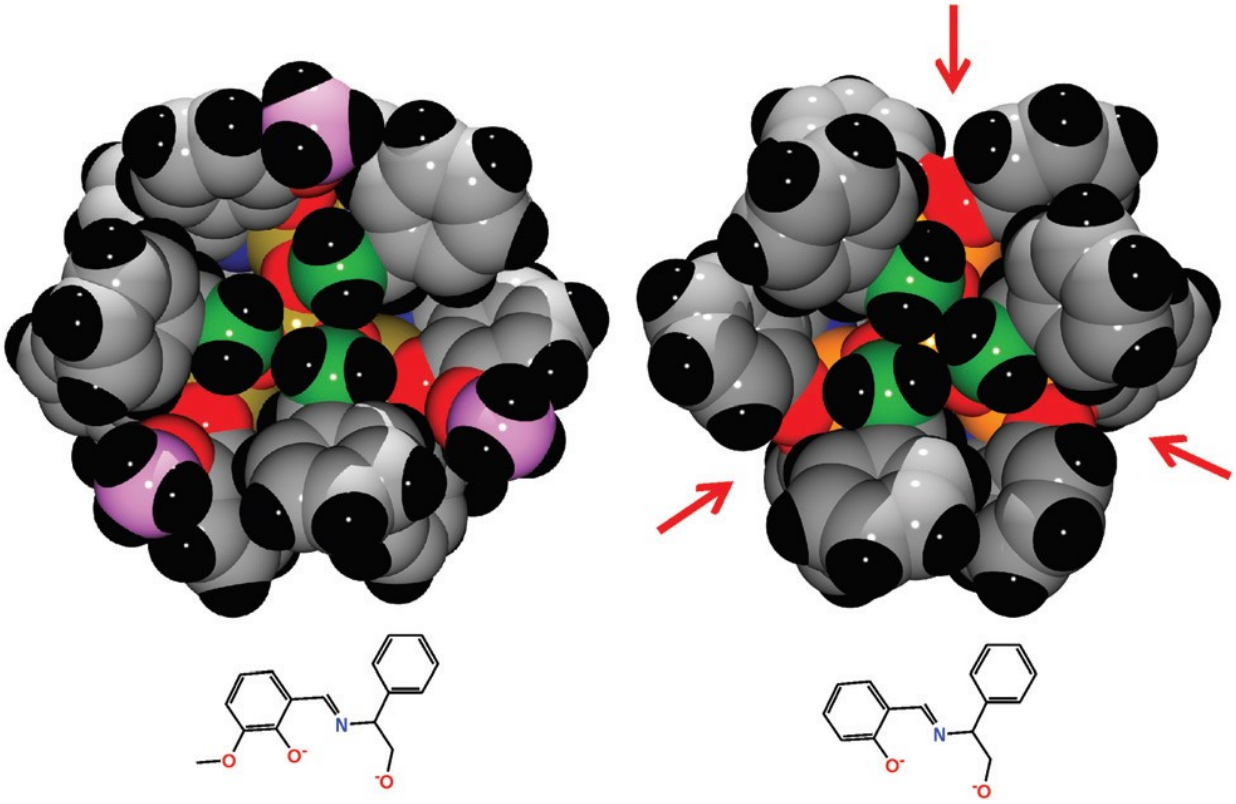

546

547

548 **FIGURE 4**

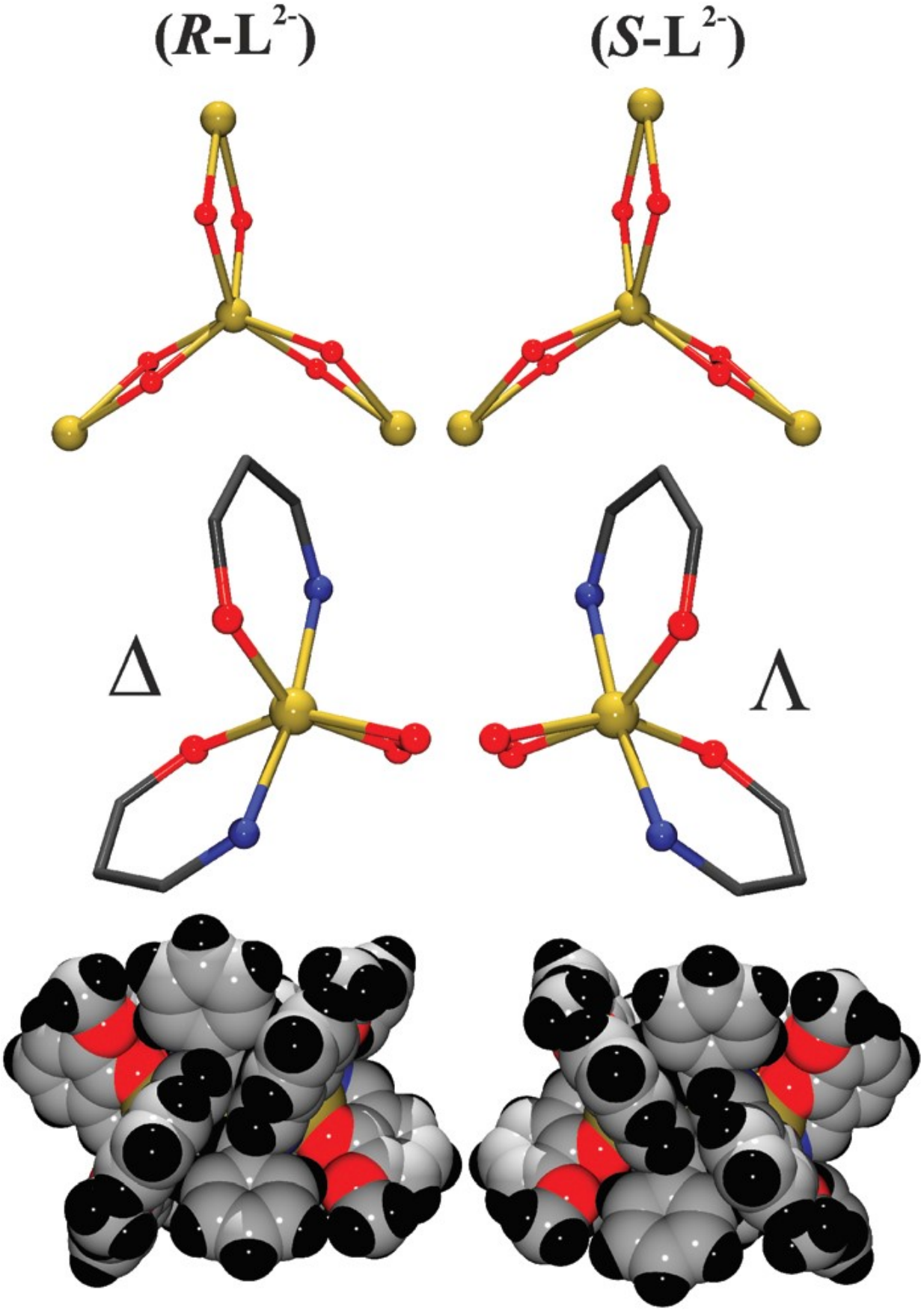

549

550

551 **FIGURE 5**

552

553

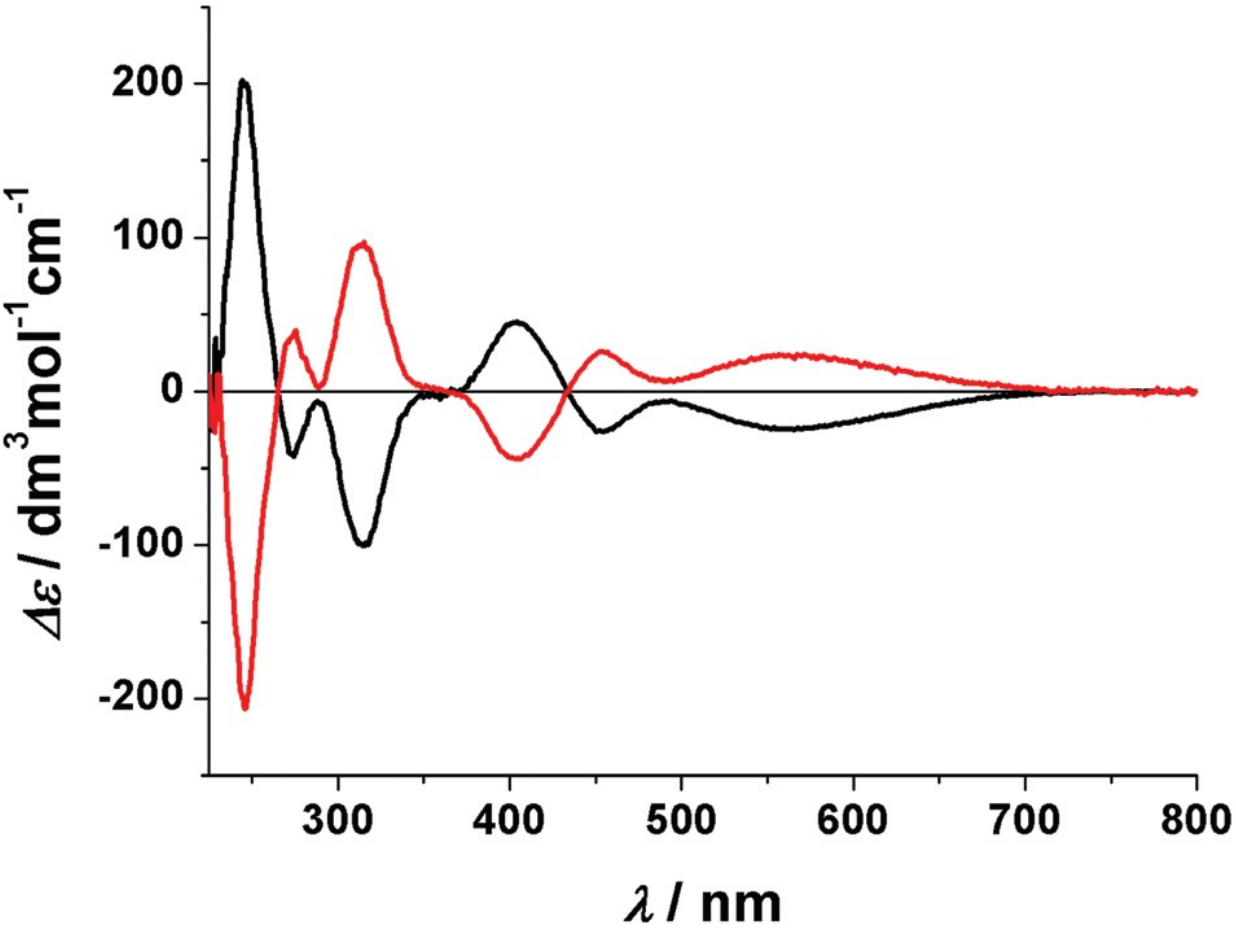

554

555

556 **FIGURE 6**

557

558

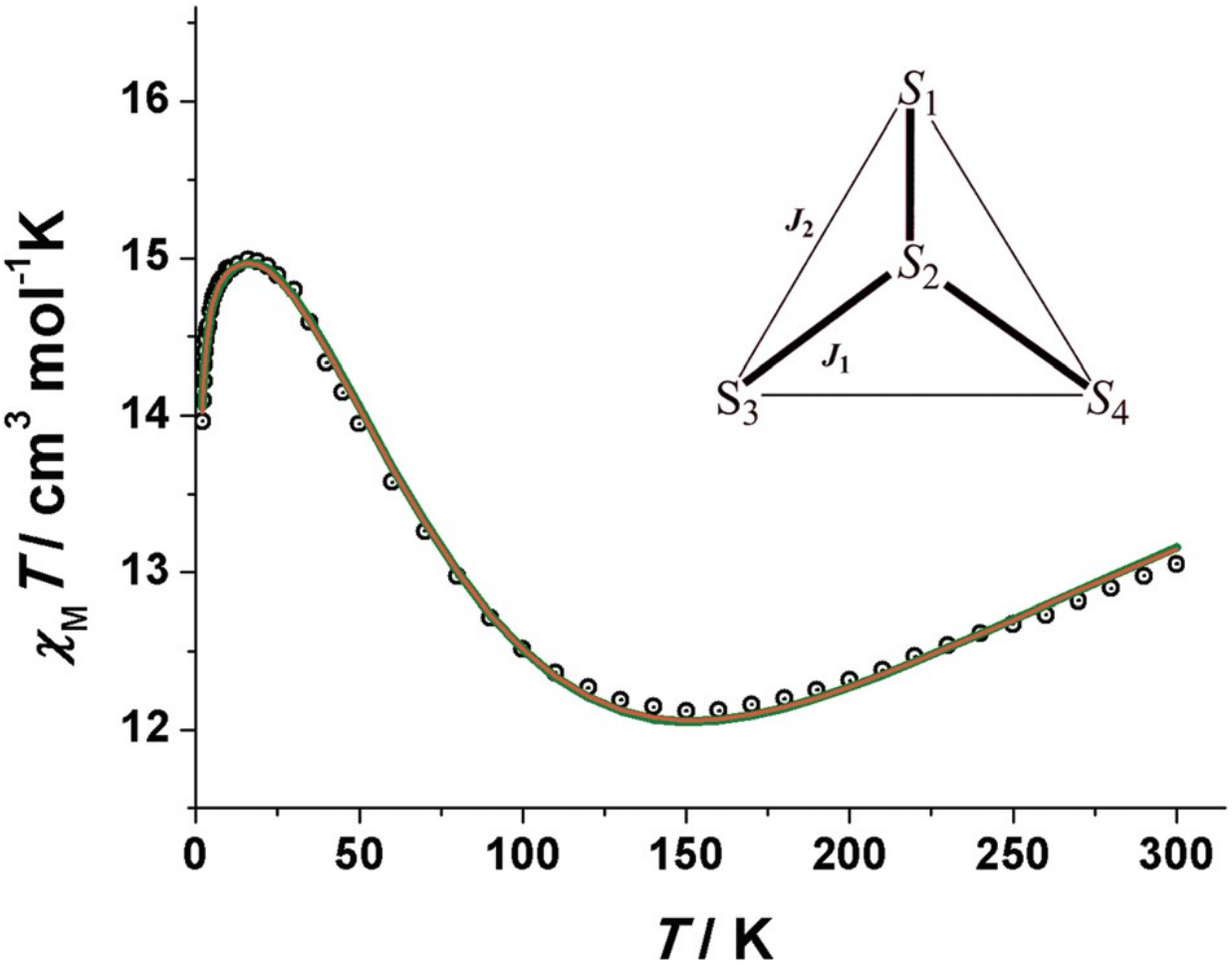

559

560

561 **FIGURE 7**

562

563

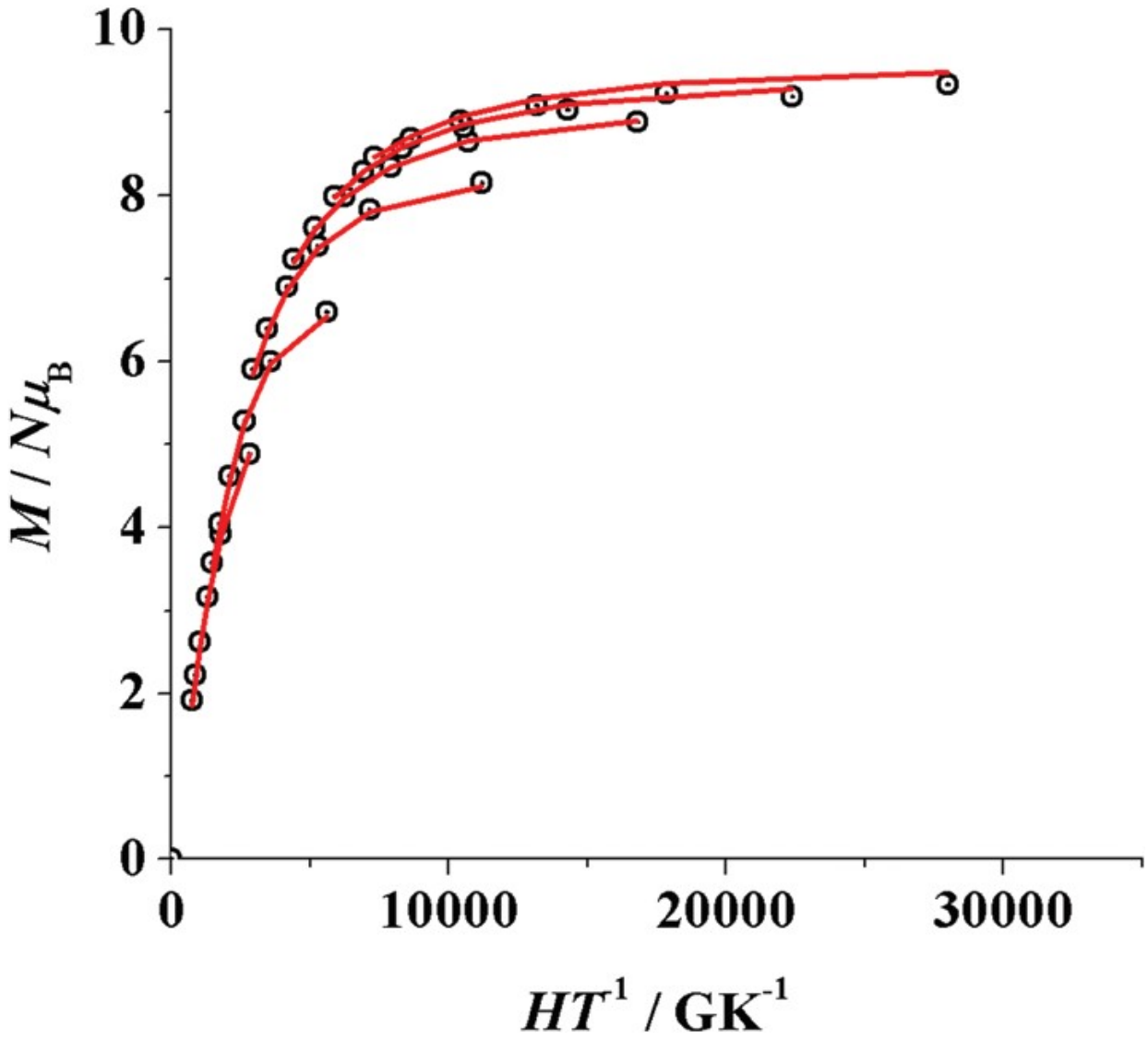

564

565

FIGURE 8

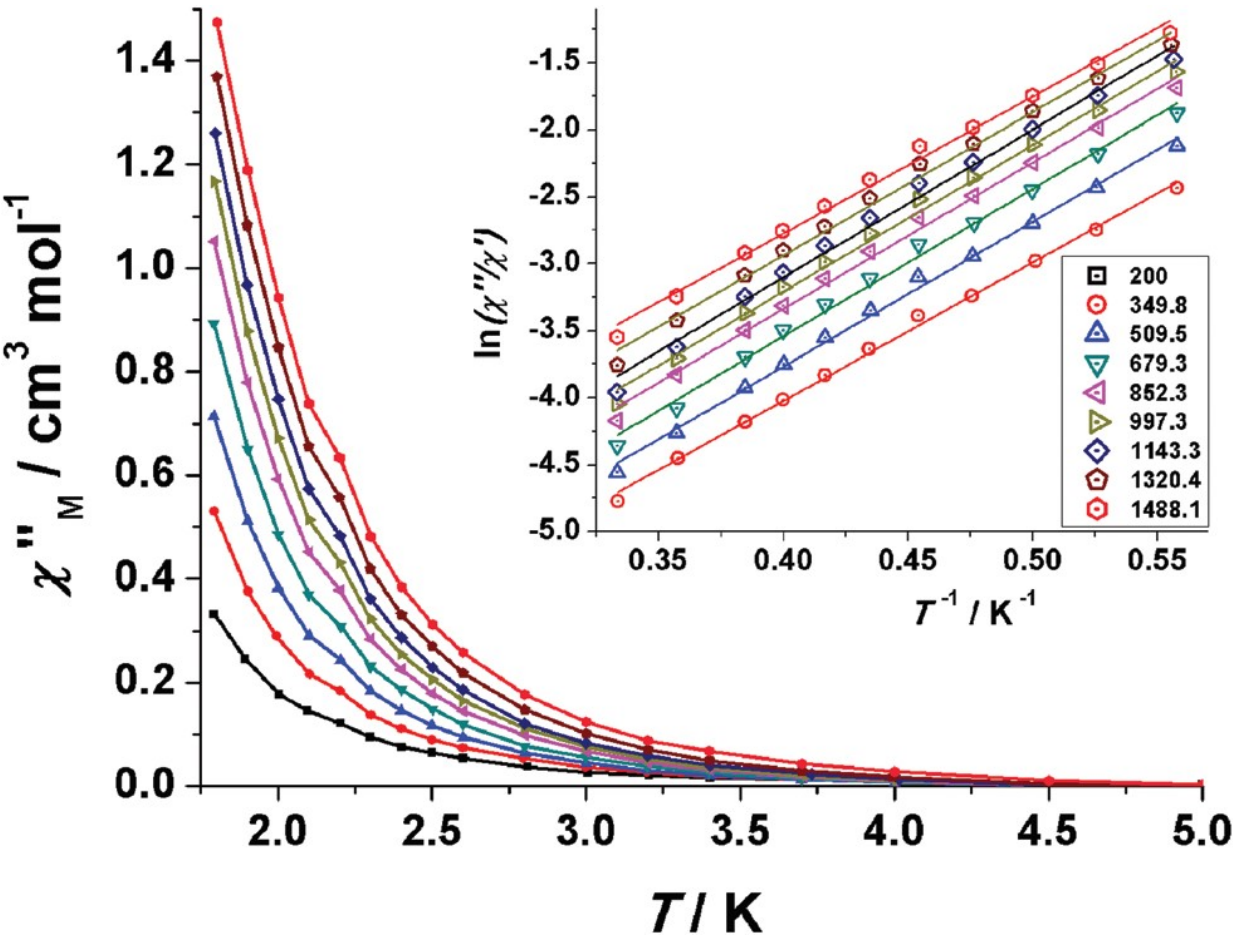
χ''M / cm3 mol-1
T / K
ln(χ''/χ')
T-1 / K-1
200
349.8
509.5
679.3
852.3
997.3
1143.3
1320.4
1488.1

SCHEME 2

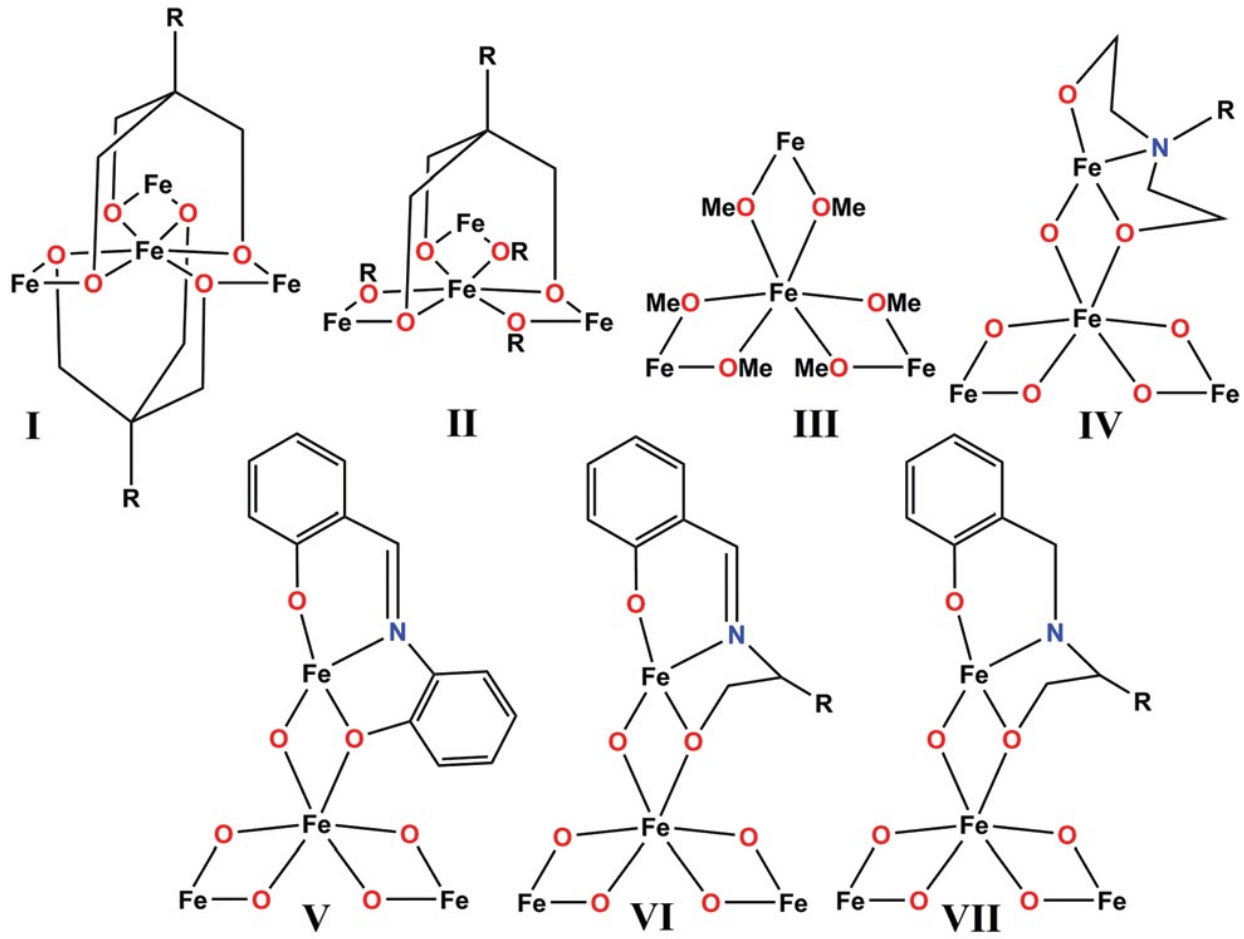

576 **FIGURE 9**

577

578

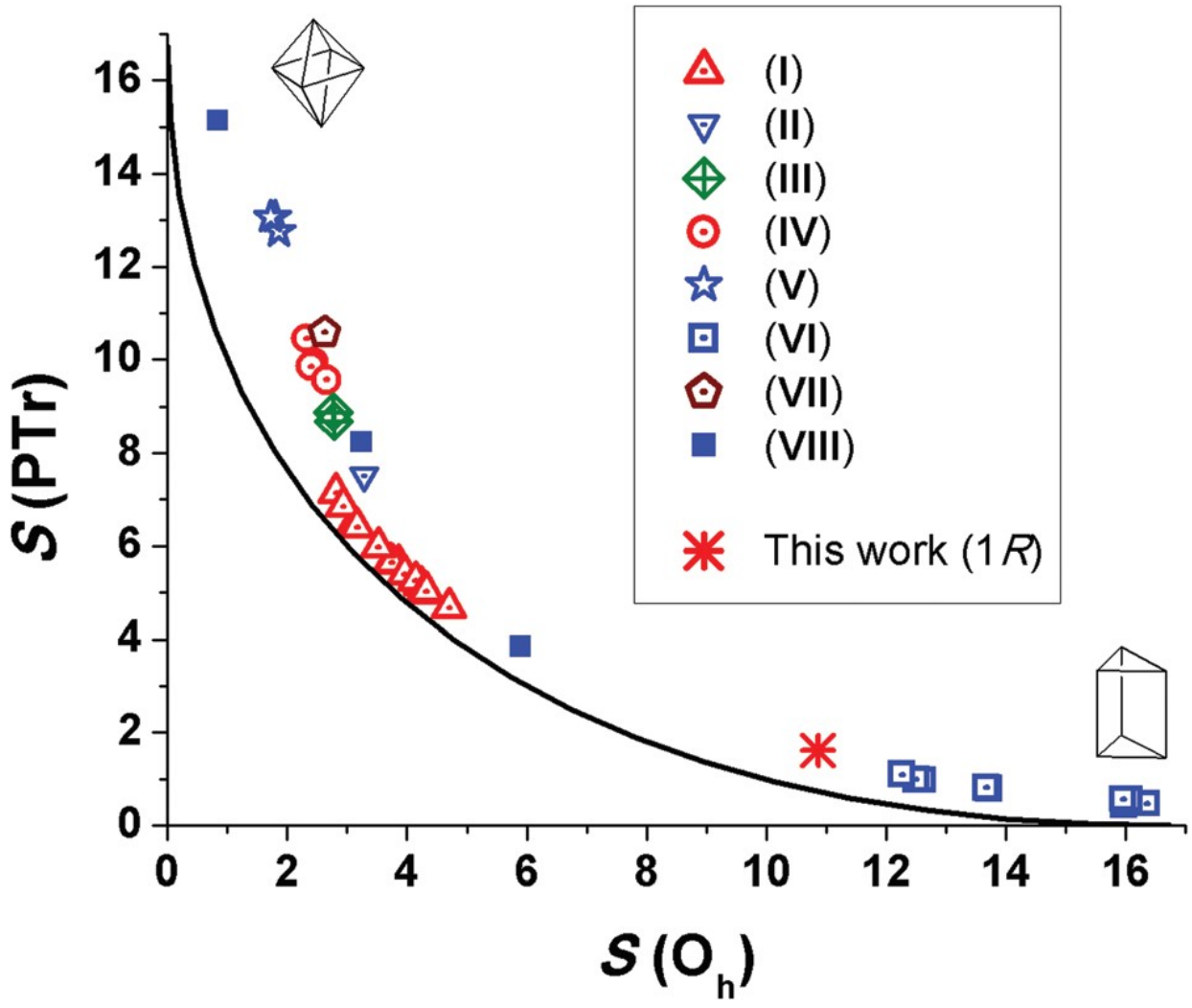

579

580

581 **FIGURE 10**

582

583

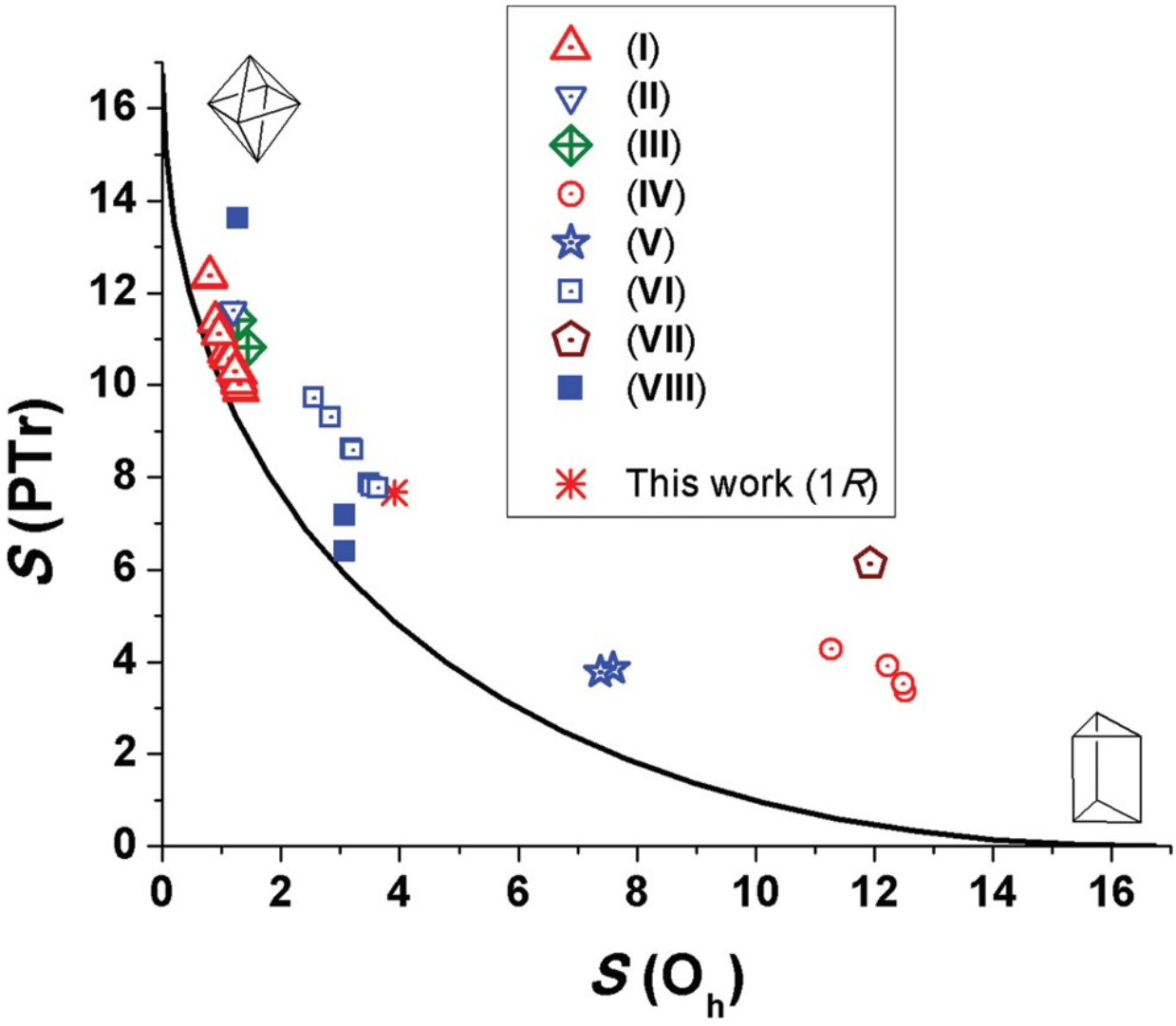

584

585

586 **FIGURE 11**

587

588

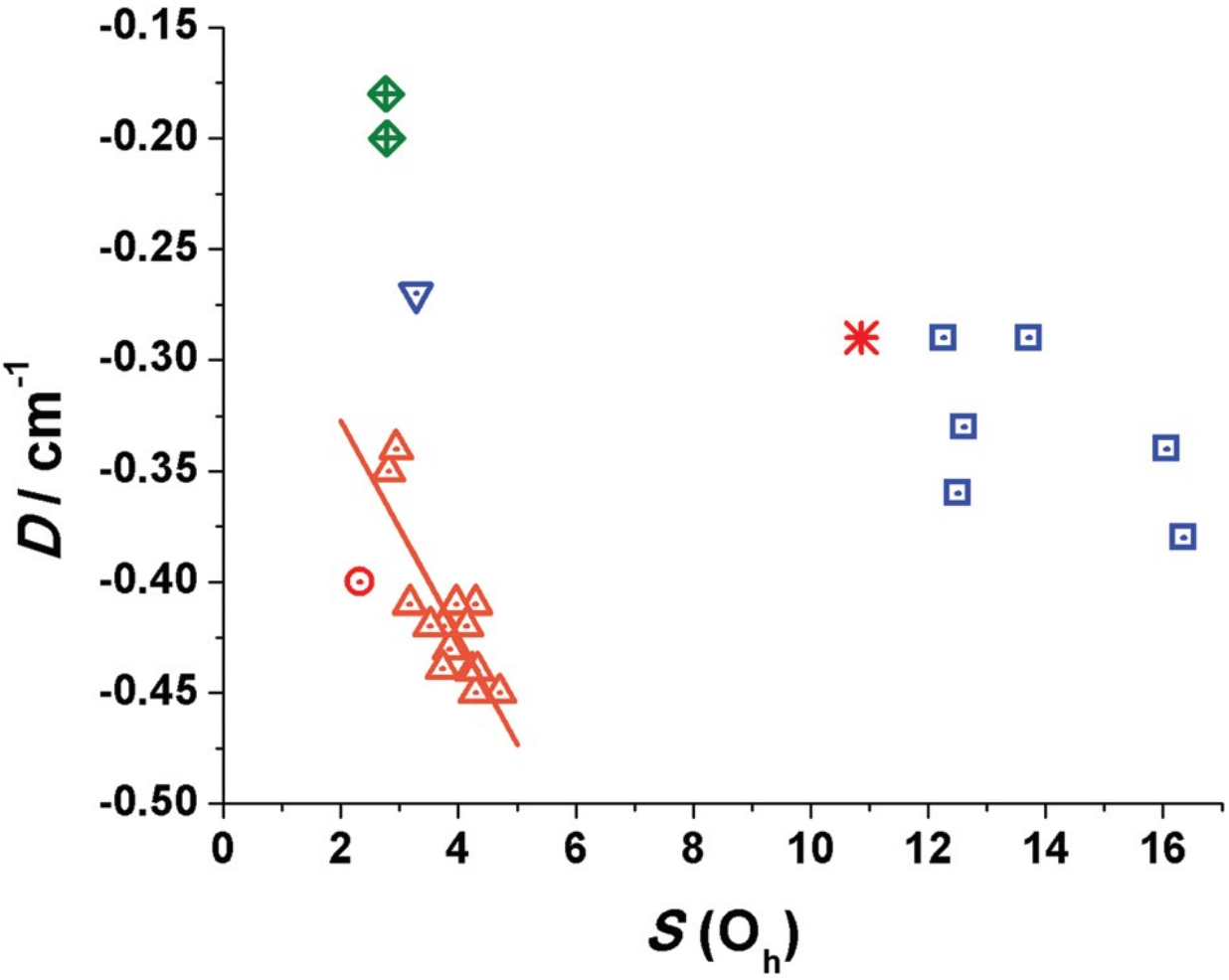

589

590

Table 1 Crystal data, collection and structure refinement details for the X-ray structure determination of complexes 1R, 1S and 2RS

	1*R*	**1*S***	**2*RS***
Formula	$C_{98}H_{94}Cl_4Fe_4N_6O_{12}$	$C_{100}H_{96}Fe_4N_6O_{12}$	$C_{49}H_{49}FeN_4O_7$
FW	2008.99	1921.24	861.77
System	Monoclinic	Monoclinic	Monoclinic
Space group	*P*21	*P*21	*P*21
a/Å	12.1916(5)	12.2369(6)	10.7824(6)
b/Å	27.895(1)	27.772(2)	18.1395(8)
c/Å	14.2943(6)	14.252(1)	11.3010(6)
α/°	90	90	90
β/°	111.665(2)	112.288(2)	99.806(2)
γ/°	90	90	90
V/Å^3	4517.9(3)	4481.7(5)	2178.0(2)
Z	2	2	2
T/K	100(2)	100(2)	100(2)
θ range/°	2.316–26.467	2.321–26.459	2.662–23.859
Reflex. collected	60409	145485	22062
Reflex. indep.	18333	18383	6642
Parameters	1171	1179	554
λ(MoKα)/Å	0.71073	0.71073	0.71073
ρ_{calc}/g cm^{-3}	1.477	1.424	1.314
μ(MoK_α)/ mm^{-1}	0.822	0.710	0.403
Flack parameter	0.011(4)	0.004(3)	0.009(4)
R	0.0515	0.0331	0.0228
ωR^2	0.1391	0.0750	0.0553

595 **Table 2** Main bond distances (Å) and angles (°) for complex 1S

596

Fe2–O1	2.075(2)	Fe3–O7	2.001(3)
Fe2–O4	1.984(2)	Fe3–O8	1.934(3)
Fe2–O7	2.011(3)	Fe3–O10	2.001(3)
Fe2–O10	2.020(2)	Fe3–O11	1.924(3)
Fe2–O13	1.998(3)	Fe3–N3	2.114(3)
Fe2–O16	2.040(3)	Fe3–N4	2.115(3)
Fe1–O1	2.001(3)	Fe4–O13	2.016(3)
Fe1–O2	1.924(3)	Fe4–O14	1.925(3)
Fe1–O4	2.016(3)	Fe4–O16	2.000(3)
Fe1–O5	1.927(3)	Fe4–O17	1.927(3)
Fe1–N1	2.136(3)	Fe4–N5	2.158(3)
Fe1–N2	2.136(3)	Fe4–N6	2.159(3)
Fe2–O1–Fe1	104.4(1)	Fe2–O13–Fe4	109.0(1)
Fe2–O4–Fe1	107.3(1)	Fe2–O16–Fe4	108.0(1)
Fe2–O7–Fe3	104.1(1)		
Fe2–O10–Fe3	104.8(1)		

597

598

599 **Table 3** Main coupling constant and range of structural parameters for the reported Fe4 complexes

600

CCDC CODE	Type	J^c	Fe–O–Fe[d] (°)	Fe–O[d] (Å)	D (cm^{-1})	U_{eff} (K)	AC peaks	Ref.
AGAQIJ	I	−16.2	102.1–103.3	1.976–1.996	−0.43[a,b]	15.7	>2 K	5
DUFNUO	I	−17	101.8–102.4	1.960–1.984	−0.35[a]	12.6	<2 K	8 and 9
DUFPAW	I	−16.4	101.6–102.6	1.977–1.983	−0.34[a]	12.2	<2 K	8 and 9
DUPSAK	I	−15.9	101.9–102.6	1.963–1.992	−0.439[a]	14.9/17.2	>2 K	12
ICOCIN	I	−15.3	102.0–102.4	1.972–1.981	−0.42[b]	15.6	>2 K	2
ITAKUJ	I	−16.5	102.8–103.0	1.963–1.983	−0.45[a,b]	17	>2 K	1
KAXGUN	I	−16.9	101.9–102.6	1.970–1.989	−0.42[a,b]	15.0	>2 K	11
NIPJEC	I	−16.9	102.2–103.0	1.970–1.983	−0.45[a]–0.43[b]	15.9	>2 K	3
TACFUA	I	−13.7	102.1–102.4	1.968–1991	−0.407[a] 0.414[b]	11.1	>2 K	10
TACGAH	I	−16.7	101.8–102.6	1.970–1.993	−0.403[a]–0.421[b]	11.14	>2 K	10
VOBXUG	I	−16	101.6–102.6	1.972–1.994	−0.42[a]–0.41[b]	—	—	4
XUBVUM	I	−17.7	102.0–103.2	1.965–1.995	−0.42[b]	15.9	>2 K	7
XUBWAT	I	−17.2	102.1–102.8	1.967–1.997	−0.45[b]	11.9	>2 K	7
XUBWEX	I	−15.6	102.2–103.0	1.961–2.005	−0.44[b]	12.9/9.5	>2 K	7
XUBWIB	I	−15.9	101.4–101.9	1.973–1.988	−0.41[b]	16.1	>2 K	7
ICOCOT	II	−21.4	103.0–105.5	1.938–2.016	−0.27[a]	6.0	<2 K	2
DEKPAK	III	−21.1	104.3–104.4	1.950–2.016	−0.20[a,b]	3.5	<0.8 K	14
GANWEA	III	−17.9	104.4–105.0	1.952–2.011	−0.18[a]	—	—	15
MEMKAR	IV	−20.8	105.1–106.7	1.982–2.030	−0.40[b]	—	—	17
CUHJEW	V	−15.7	106.0–107.1	1.997–2.098	—	—	—	19
JORWAQ	VI	−23.4	105.6	2.003–2.021	−0.38[a]–0.37[b]	14.1	<2 K	22
UVIPUL	VI	−23.6	105.3–107.4	2.014–2.041	−0.34[a]	5.9/9.9	<2 K	21
XOKDEI	VI	−24.8	105.1–107.1	1.993–2.049	−0.33[a]	7.0	<2 K	23
XOKDIM	VI	−23.2	104.9–107.5	1.982–2.047	−0.36[a]	11.0	<2 K	23
XOKDOS	VI	−26.4	105.5–107.2	1.992–2.052	−0.29[a]	—	<0.5	23
XOKQAR	VI	−22.8	105.6–108.0	2.003–2.046	−0.29[a]	—	<0.5	23
1*S*	VI	−19.0	104.1–109.0	1.924–2.075	−0.29[a]	15.4 K	<2 K	This work
AHOTEX	VII	−21.9	107.2–108.5	1.970–2.009	~0[a]	—	<1.8 K	24
DAMREQ	VIII	−5.5	99.9–101.0	2.030–2.045	—	—	—	25
GAGREM	VIII	−28.2	105.0–105.3	1.984–1.995	−0.32[a]–0.33[b]	8.5	<0.8 K	13
LEBRIU	VIII	−29.2	104.4–107.1	1.942–2.050	−0.31[a]	—	NO	26

[a] Value calculated from reduced magnetization measurements. [b] Value calculated from EPR data. [c] Referred to the $H = JS_iS_j$ convention. [d] Maximum and minimum value for each parameter.

601